Elastic scattering of protons from ^{11}Li and the neutron halo

A. N. F. Aleixo and C. A. Bertulani
Instituto de Física, Universidade Federal de Rio de Janeiro, 21945 Rio de Janeiro, Rio de Janeiro, Brazil

M. S. Hussein
Instituto de Física, Universidade de São Paulo, Caixa Postal 20516, 01498 São Paulo, São Paulo, Brazil
(Received 22 October 1990)

The elastic-scattering angular distribution of $p+^{11}$Li at $E_{\rm lab}=100$ MeV is evaluated within Glauber's theory. The p-^{11}Li optical potential is evaluated within the "$t\rho$" approximation with $\rho_{^{11}\rm Li}$, the matter density of ^{11}Li, calculated within constrained Hartree-Fock theory. Medium effects on the nucleon-nucleon t matrix, are fully taken into account. The effect of the halo neutrons on $d\sigma/d\Omega$ is assessed through comparison with the $p+^{12}$C and $p+^{9}$Li systems at $E_{\rm lab}=100$ and 800 MeV.

I. INTRODUCTION

It is clear by now that neutron- or proton-rich nuclei are intrinsically, qualitatively different many-body systems from normal stable nuclei. Both the mean-field aspects as well as the nature of the correlations among the nucleons are apparently quite different in the two systems. Nonelastic reactions, e.g., fragmentation and single neutron emission, have been reported and show clear indication of the existence of a halo.[1,2] Further tests of the halo hypothesis are certainly needed to settle the question.

The most simple process, elastic scattering, however, has not been measured. This basically stems from the low current of the secondary beam, namely, e.g., ^{11}Li. Recently it has been reported that elastic angular distribution of ^{11}Li from hydrogen is being accomplished at much lower energies (100 MeV/nucleon).[3] It is therefore of interest to do a preliminary qualitative calculation to assess the importance of the halo in the elastic angular distribution. Recent study of this question in the context of heavy ions has been made with the major conclusion being that systems such as ^{11}Li+^{12}C behave in a much the same way as, e.g., ^{12}C+^{12}C.[4] Stronger refractive effects were found for ^{11}Li+^{12}C. The purpose of the present paper is to extend the study of Ref. 4 to the much simpler system $p+^{11}$Li. Would the halo also bring in more refraction or, rather, long-range absorption dictates the scenario? This is the question we address ourselves to here.

Our study is based on the Glauber theory with the optical potential determined from the usual multiple-scattering series with medium effects fully taken into account. In Sec. II we present the theoretical ingredients that go into the calculations together with a convenient near-far decomposition.[5] We also introduce, as is done in Ref. 6, the momentum-transfer function. In Sec. III we present the results of our calculation for $p+^{11}$Li, $p+^{9}$Li, and $p+^{12}$C at $E_{\rm lab}=800$ MeV. We also study the case at $E_{\rm lab}=100$ MeV. In Sec. IV we give our concluding remarks. We should remark here that the Glauber theory has been applied quite successfully to describe the elastic and inelastic scattering of nuclear systems at $E_{\rm lab}<100$ MeV.[7] This should give us confidence in using this theory for our purposes here.

II. NEAR-FAR GLAUBER THEORY OF THE ELASTIC ANGULAR DISTRIBUTION

Ignoring spin-orbit effects, the Glauber amplitude that describes elastic scattering is given by

$$f(\theta)=-ik\int_0^\infty db\, bJ_0(2kb\sin(\theta/2))(e^{i\chi(b)}-1)\ , \tag{1}$$

where $k^2=(2m/\hbar^2)E$, J_0 is the ordinary Bessel function of order zero 0, b is the impact parameter, and $\chi(b)$ is the overall scattering phase given by

$$\chi(b)=-\frac{k}{E}\int_0^\infty dz\, U_N[(b^2+z^2)^{1/2}]+\chi_c(b)\ ,$$
$$\chi_C(b)=2\frac{z_T}{\hbar v}\ln(kb)\ . \tag{2}$$

In Eq. (2), U_N is the complex nuclear optical potential, χ_C is the Coulomb phase, z_T is the target charge number, and v is the relative velocity.

We now employ the relation

$$J_0(qb)=\tfrac{1}{2}[H_0^{(1)}(qb)+H_0^{(2)}(qb)]\ , \tag{3}$$

where $H_0^{1(2)}(qb)$ are Hankel functions of zero order of the first and second type, respectively. Asymtotically, these functions behave as

$$H_0^{1(2)}(x)\underset{x\gg1}{\rightarrow}\left[\frac{2}{\pi x}\right]^{1/2}\exp[+(-)i(x-\tfrac{1}{4}\pi)]\ . \tag{4}$$

In Eq. (3), q is the momentum transfer given by

$2k \sin(\theta/2)$. With (3) we can now rewrite Eq. (1) as

$$f(\theta)=f^{(+)}(\theta)+f^{(-)}(\theta) ,$$

$$f^{+(-)}_{(\theta)}(\theta)=\tfrac{1}{2}(-ik)\int_0^\infty db\, bH^{1(2)}(qb)(e^{i\chi(b)}-1) . \quad (5)$$

We refer to $f^{(+)}$ as the near-side and $f^{(-)}$ the far-side contribution to f, respectively.[5] This nomenclature is common in heavy-ion science and is also utilized by Amado and his collaborators[8] in proton-nucleus scattering.

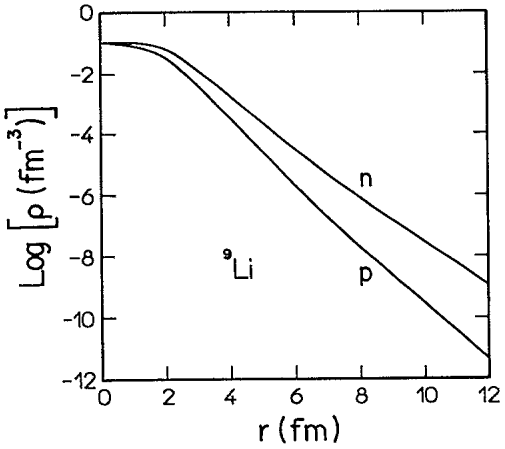

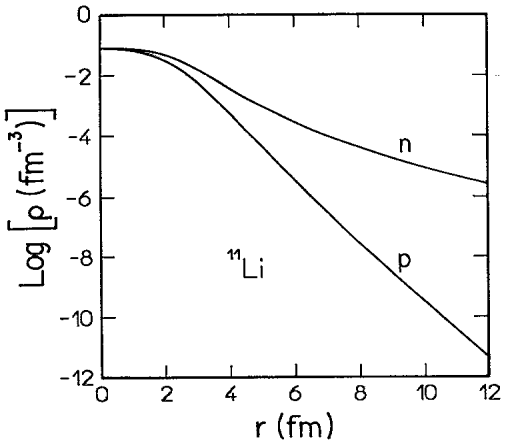

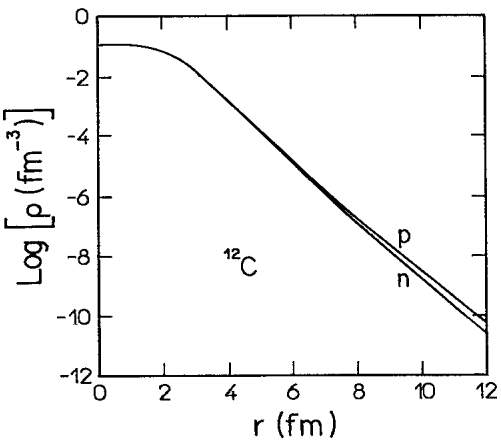

FIG. 1. The Hartree-Fock densities of neutrons and protons for (a) ^{9}Li, (b) ^{11}Li, and (c) ^{12}C (Ref. 9).

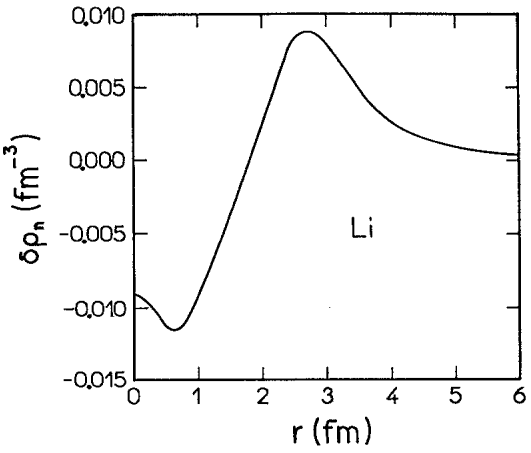

FIG. 2. The difference $\rho_n^{^{11}\mathrm{Li}}-\rho_n^{^9\mathrm{Li}}$ vs r.

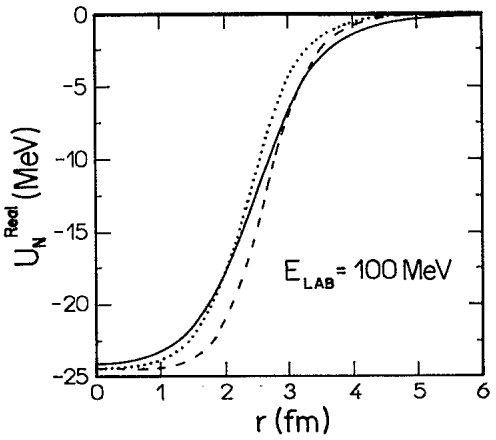

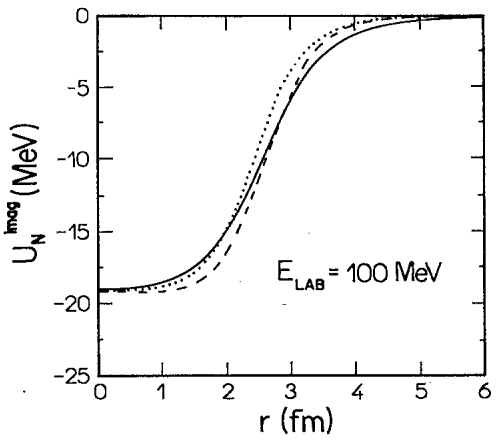

FIG. 3. The "$t\rho$" optical potential for $p+^9$Li, $p+^{11}$Li, and $p+^{12}$C at $E_{\mathrm{lab}}=100$ MeV. (a) [3(b)] displays the real (imaginary) part of the optical potential.

Whereas Amado *et al.* use Eq. (5) to obtain analytical results starting from a presumed normal thin skinned nuclear densities that enter into the construction of $\chi(b)$ (see discussion below), we opt here for a simple numerical evaluation of $f^{(+)}$ and $f^{(-)}$ since the exotic nucleus discussed here, namely, ^{11}Li, has surface diffuseness even larger than the radius.

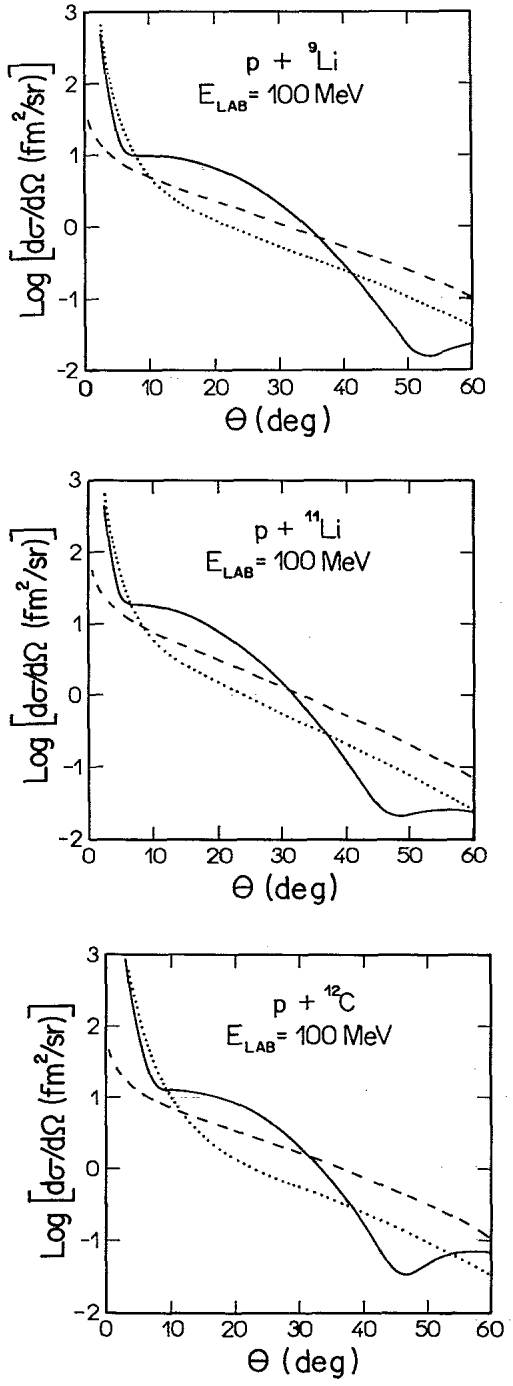

FIG. 4. The elastic-scattering differential cross section versus center-of-mass angle for (a) $p+^{9}$Li (b) $p+^{11}$Li, and (c) $p+^{12}$C at $E_{lab}=100$ MeV. Also shown are the near (dotted curve) and far (dashed curve) contributions.

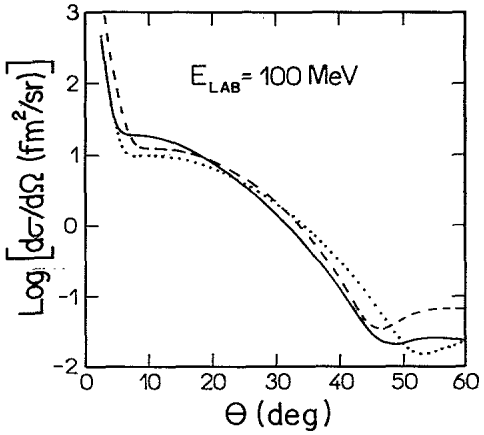

FIG. 5. The elastic cross sections for the three systems: $p+^{9}$Li (dotted), $p+^{12}$C (dashed), and $p+^{11}$Li (solid).

Before presenting our results, it is useful to further analyze the amplitudes $f^{(+)}$ and $f^{(-)}$. At energies $E \gtrsim 100$ MeV, it is expected that $\chi(b)$ becomes reasonably large. Thus, the amplitudes $f^{(+)}$ and $f^{(-)}$ could be dominated by the stationary phase contributions b_s^+ and b_s^- determined from Eq. (2):

$$\pm q = \frac{d}{db}\chi(b)|_{b_s^\pm} . \tag{6}$$

Equation (6) can be written as [see Eq. (2)]

$$\pm q = -\frac{k}{E}\int_0^\infty dz \frac{b_s}{(b_s^2+z^2)^{1/2}} \frac{dU_N[(b_s^2+z^2)^{1/2}]}{d(b_s^2+z^2)^{1/2}} + \frac{2z_T e^2}{\hbar v}\frac{1}{b_s} \tag{7}$$

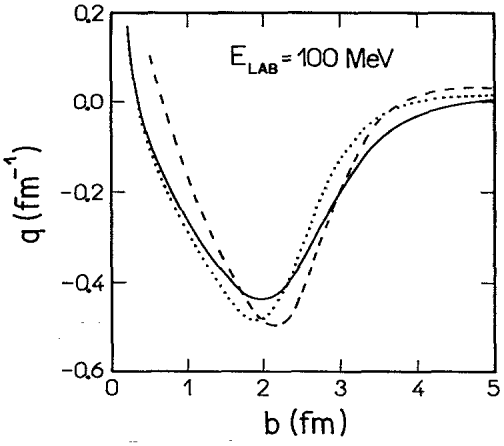

FIG. 6. The momentum-transfer function $q(b(\theta))$ for the three systems studied. The solid line is for ^{11}Li, the dotted line is for ^{9}Li, and the dashed line is for ^{12}C.

for $b_s^{\pm}$. At this point we remind the reader that $\pm q$ corresponds to $2k \sin(\pm\frac{1}{2}\theta)$, thus Eq. (7) dictates the angular region where $f^{(+)}$ and $f^{(-)}$ are dominant. Clearly, both b_s^+ and b_s^- are complex, owing to the complex nature of U_N and to the possibility of being in a classically forbidden angular region.[5]

Before proceeding in the presentation of our numerical results, we should mention that spin-polarization observables are very useful in shedding more light on the interaction. The discussion of spin polarization in $p + ^{11}$Li is, however, complicated by the high-spin value of the ^{11}Li ground state ($\frac{3}{2}$). This makes the analysis rather involved and we opt here to leave this for a future work.

III. THE ELASTIC SCATTERING OF $p + ^{11}$Li, $p + ^{9}$Li, and $p + ^{12}$C

In this section, we apply the formalism developed in the previous section to the elastic scattering, of $p + ^{11}$Li and compare it to that of $p + ^{9}$Li and $p + ^{12}$C. We choose the laboratory energy to be 100 MeV. Our aim here is to assess the qualitative effect of the neutron halo in ^{11}Li on the angular distribution. To further understand the phenomenon, we also make the comparison at $E_{\rm lab} = 800$ MeV.

In Fig. 1 we show the calculated proton and neutron densities for ^{9}Li, ^{11}Li, and ^{12}C. These results were taken from the Hartree-Fock calculation of Bertsch *et al.*[9] To clearly exhibit the spatial extent of the two valence neutrons (in the $1P_{1/2}$ level) in ^{11}Li, we show in Fig. 2 the difference $\delta\rho_n \equiv \rho_n^{^{11}\rm Li} - \rho_n^{^{9}\rm Li}$. It is clear that the two valence neutrons contribute to the density in the region $2 < r < 5$ fm. Notice that, at $r < 2$ fm, the contribution is negative. Further, the matter radius of ^{9}Li is about 2.5

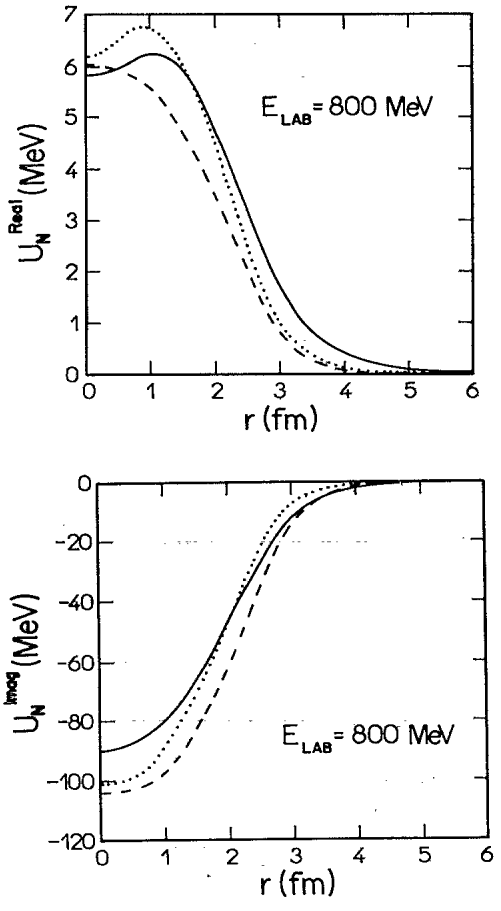

FIG. 7. Same as Fig. 3 at $E_{\rm lab} = 800$ MeV.

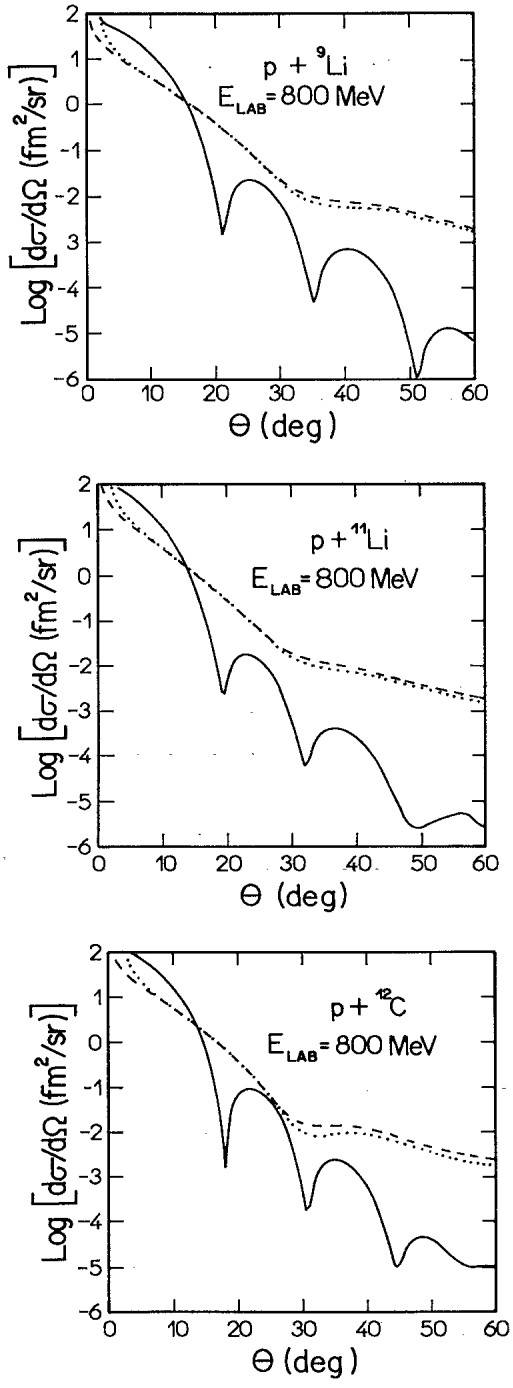

FIG. 8. Same as Fig. 4 at $E_{\rm lab} = 800$ MeV.

fm. We next construct the $p+A$ optical potential. We do this by using the $t\rho$ approximation with medium corrections. At $E_{\rm lab}=100$ MeV, the average, medium modified, nucleon-nucleon optical potential is given by[10]

$$U_N(r)=\langle t_{pn}\rangle\rho_n(r)+\langle t_{pp}\rangle\rho_p(r)\ , \tag{8}$$

where

$$t_{pN}=-\frac{E}{k}\bar{\sigma}_{pN}(\xi_{pN}+i),\quad N=p \text{ or } n\ ,$$
$$\xi_{pp}=1.87\ , \tag{9}$$
$$\xi_{pn}=1.00\ .$$

The Pauli-corrected nucleon-nucleon total cross section is given by[10]

$$\bar{\sigma}_{pN}=\sigma_{pN}(E)P\left[\frac{E_F}{E}\right]\ , \tag{10}$$

where

$$P(x)=\begin{cases}1-\frac{7}{5}x, & x\le\frac{1}{2},\\ 1-\frac{7}{5}x+\frac{2}{5}x\left[2-\frac{1}{x}\right]^{5/2}, & x\ge\frac{1}{2}\ ,\end{cases} \tag{11}$$

and

$$E_F^{(N)}=\frac{\hbar^2}{2m_N}[k_F^{(N)}]^2\ ,$$
$$k_F^{(N)}=[\tfrac{3}{2}\pi^2\rho_N(r)]^{1/3}\ , \tag{12}$$

and, finally,

$$\sigma_{pp}=33.2 \text{ bm}\ ,$$
$$\sigma_{pn}=72.7 \text{ mb}\ .$$

In Fig. 3 we show the resulting optical potential for the three systems $p+{}^9$Li, $p+{}^{11}$Li, and $p+{}^{12}$C. The real parts, shown in Fig. 3(a) look very similar except for the strength which is larger the heavier the target is, as expected from Eq. (8) and Fig. 1. However, $p+{}^{11}$Li has a much larger diffuseness, as anticipated, owing to the presence of the halo. In all cases, the real part is attractive. Similar behavior is also seen in the imaginary part of the potential as Fig. 3(b) shows.

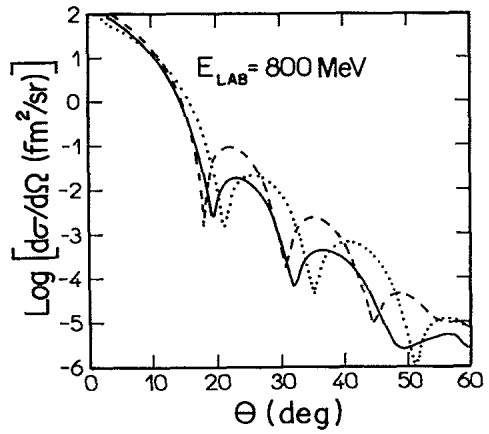

FIG. 9. Same as Fig. 5 at $E_{\rm lab}=800$ MeV.

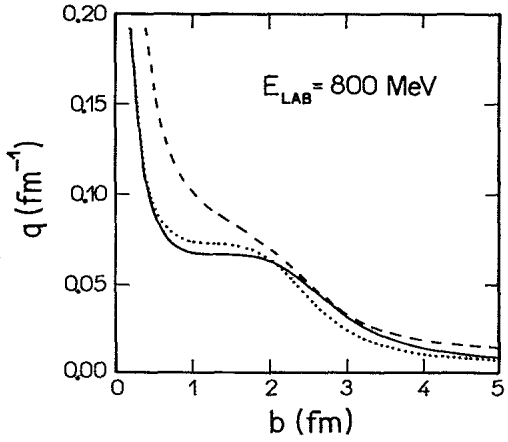

FIG. 10. Same as Fig. 6 at $E_{\rm lab}=800$ MeV.

The elastic-scattering angular distributions calculated from Eq. (1) are shown in Fig. 4. The near contribution and the far contribution to $d\sigma/d\Omega$ [Eq. (5)] are also shown individually. In all three cases, the far-side component dominates over the near-side one, at least in the $\theta>10°$ region. However, a very important qualitative change due to the relatively large size of ^{11}Li (the halo) is the fact that, in the angular region $8°<\theta<20°$, the $p+{}^{11}$Li cross section is larger than that of $p+{}^{12}$C.

This is clearly seen in Fig. 5 where the cross sections for the three systems are exhibited together. Note the position of the second minimum occurs at $\theta=53°$ in ^{9}Li, $\theta=47°$ in ^{11}Li, and $\theta=46°$ in ^{12}C, clearly showing the influence of the greater extention of the matter distribution in ^{11}Li. The above features should be easily tested experimentally.

To further understand the nature of the scattering, we have also calculated the momentum-transfer function $q(b(\theta))$ of Eq. (7) for the three systems. This function, in the Glauber theory, has a similar role to the classical deflection function extensively studied in the semiclassical treatment of scattering, e.g., of heavy ions. In Fig. 6 we show the real part of $q(b(\theta))$ vs b for the three systems under study. Again, whereas the region $0<b<3$ fm is as expected from general nuclear systematics, the region $b>3$ fm clearly exhibits the effect of the halo. Appreciably larger impact parameters seem to contribute to the scattering of $p+{}^{11}$Li than of $p+{}^9$Li and $p+{}^{12}$C for a given value of the momentum transfer (angle).

To complete the comparison among the three systems, we performed the elastic-scattering calculation at $E_{\rm lab}=800$ MeV/nucleon. Although the experiment at this energy is very difficult, owing to the very low current of the ^{11}Li secondary beam, we felt that such a comparison would further illucidate the question of the neutron halo. Thus, in Figs. 7–10, we present the corresponding "$t\rho$" optical potential, the elastic-scattering angular distribution with its near-far decomposition, the three cross

TABLE I. Total reaction cross section for the system $p+X$.

X	E (MeV)	σ_R (mb)
^{12}C	100	172
	800	178
^{11}Li	100	219
	800	183
^{9}Li	100	153
	800	140

sections, and the momentum-transfer functions, respectively. The nucleon-nucleon total cross sections and the parameters ξ_{PN} used in the calculation were taken from the literature[10] and are $\sigma_{pp}=47.3$ mb, $\sigma_{pn}=37.9$ mb, $\xi_{pp}=0.06$, and $\xi_{pn}=-0.2$.

At $E_{\rm lab}=800$ MeV/nucleon, the real part of the "$t\rho$" optical potential is repulsive and the imaginary part is quite strong (Fig. 7). The momentum-transfer function emphasizes this point in Fig. 10. This favors a situation of almost equality between the near and far contributions to $d\sigma/d\Omega$. The resulting Fraunhofer pattern is clearly seen in Fig. 9 for the three systems. Unfortunately, at this higher energy, the change in the oscillatory pattern of $d\sigma/d\Omega$ arising from the neutron halo is very small, making its study at this energy quite difficult. Finally, to complete the comparison between the three systems, we present the values of the total reaction cross section σ_R at the two energies considered in Table I. Although σ_R for $p+^{11}$Li is larger than that of $p+^{9}$Li and $p+^{12}$C at both energies, the trend with energy, namely,

$$\sigma_R(E_{\rm lab}=800\ {\rm MeV})<\sigma_R(E_{\rm lab}=100\ {\rm MeV})\ ,$$

is fully understood from the general behavior of σ_{NN} and nuclear transparency.[10] Notice that, for $p+^{12}$C, $\sigma_R(800\ {\rm MeV})\sim\sigma_R(100\ {\rm MeV})$.

IV. DISCUSSION AND CONCLUSIONS

In this paper, the elastic-scattering angular distribution of the "exotic" system $p+^{11}$Li is studied at $E_{\rm lab}=100$ and 800 MeV, and is compared to the normal systems $p+^{9}$Li and $p+^{12}$C. The qualitative and quantitative changes that the two-neutron halo in ^{11}Li inflicts on the elastic angular distribution is assessed. It is emphasized that lower-energy data such as those planned by Tanihata[3] at $E_{\rm lab}=100$ MeV should clearly exhibit the phenomenon.

Supported in part by Conselho Nacional de Desenvolvimento Cientifico e Technológico (CNPq) and Fundacaño de Amparo e Pesquisa do Estado de Saño Paulo (FAPESP), São Paulo, Brazil.

[1]I. Tanihata *et al.*, Phys. Lett. **160B**, 380 (1985); Phys. Rev. Lett. **55**, 2676 (1985); Phys. Lett. B **206**, 592 (1988)
[2]T. Kobayashi *et al.*, Phys. Lett. B **232**, 51 (1989); C. A. Bertulani and M. S. Hussein, Phys. Rev. Lett. **64**, 1099 (1990).
[3]I. Tanihata, private communication.
[4]G. R. Satchler, K. W. McVoy, and M. S. Hussein, Nucl. Phys. **A522**, 621 (1991).
[5]M. S. Hussein and K. W. McVoy, Prog. Part. Nucl. Phys. **12**, 103 (1984).
[6]B. V. Carlson, M. P. Isidro Filho, and M. S. Hussein, Phys. Lett. **154B**, 89 (1985).
[7]A. Vitturi and F. Zardi, Phys. Rev. C **36**, 1404 (1987); S. M. Lenzi, A. Vitturi, and F. Zardi, *ibid.* **38**, 2086 (1988); **40**, 2114 (1989); S. M. Lenzi, F. Zardi, and A. Vitturi, *ibid.* **42**, 2079 (1990).
[8]R. D. Amado, in *Advances in Nuclear Physics,* edited by J. W. Negele and E. Vogt (Plenum, New York, 1985), Vol. 15.
[9]G. F. Bertsch, B. A. Brown, and H. Sagawa, Phys. Rev. C **39**, 1154 (1989).
[10]M. S. Hussein, R. A. Rego, and C. A. Bertulani, Phys. Rep. (in press).